

# Plasma and metastable distributions in low pressure Ar and He discharges

M. R. Talukder, S. Bose and M. Kando<sup>a)</sup>

*Department of Applied Physics & Elec. Eng., University of Rajshahi, Rajshahi-6205, Bangladesh.*

*<sup>a)</sup>Graduate School of Electronic Science and Technology, Shizuoka University, 3-5-1 Johoku, Hamamatsu 432-8011, Japan.*

Probe characteristics were measured, under metastable induced secondary electron emission (SEE) condition from the probe surface, in low-pressure microwave excited Ar and He discharge plasmas. Collected and emitted currents were, extracted from the total probe currents, used to determine plasma parameters and metastables density. It is found that electron temperature decreases with increasing pressure and axial distance, due to increasing electron-neutral collision frequency for momentum transfer and due to decreasing energy of microwave field. The densities of electrons and metastables increase with increasing pressure because of increasing ionizing and electron-neutral collisions to the metastable level frequencies by electron impact. A theoretical study was carried out to validate the experimental results. Model predictions compare favorable with the experimental results.

## 1. Introduction

Large area microwave excited plasma sources are drawing much attraction for microelectronics industries. For plasma source design, and discharge performance optimization, it is very important to know the plasma parameters, and their spatial behaviors. Langmuir probe is a widely used diagnostic tool for the determination of local plasma properties, which are difficult to determine by other diagnostic techniques. The probe characteristics measured in our experiment show increased probe currents in the lower probe potential region. It is found that this increment of current is caused by the metastable induced SEE [1] current due to the Auger neutralization of ions or Auger deexcitation of metastable atoms [2]. In order to study the spatial plasma and metastables density profiles, an effort is given to analyze the probe characteristics taking into account secondary electron emission current. Theoretical studies are carried out to predict electron temperature ( $T_e$ ), and metastable density ( $n_m$ ) as the functions of pressure ( $p$ ), distance ( $r, z$ ), and electron density ( $n_e$ ). It is found that experimental results and model predictions are encouraging.

## 2. Probe current

Secondary electrons can be emitted from the metal surface due to ion impact, electron impact, photon or de-excitation of metastable atoms. SEE due to ion impact, and photons are negligible under typical experimental conditions. For strongly positive polarized probe, the probe can be heated by the bombardment of highly energetic electrons and consequently thermionic emission may take place. To avoid probe heating, probe characteristics are measured within very short

time. However, under metastable induced SEE, the total current [3]  $I_T$  to the probe is

$$I_T = I_e - I_i - I_{em}, \quad (1)$$

where  $I_e$ ,  $I_i$ , and  $I_{em}$  are the collected electron, and ion currents, and emission current, respectively. When  $V_f \leq V_p \leq V_s$ , where  $V_f$ ,  $V_p$ , and  $V_s$  are the floating, probe and plasma potentials, respectively, then  $I_e \gg I_i$ , and Eq. (1) becomes

$$I_T = I_e - I_{em}. \quad (2)$$

For  $V_p \ll V_f$ ,  $I_e \ll I_i$ , Eq. (1) becomes

$$I_T = -I_i - I_{em}. \quad (3)$$

Eqs. (2), and (3) are used iteratively to fit the positive and the negative part of the probe data to determine plasma parameters and metastables density.

### 3.1. Estimation of $I_{em}$

The emission current is obtained [1] from

$$I_{em} = \gamma e A_p \Gamma_m, \quad (4)$$

where  $\gamma$ ,  $e$ ,  $\Gamma_m$  and  $A_p$  are the metastable induced SEE coefficient, electronic charge, the metastable flux to the probe and surface area of the probe, respectively.

### 3.2. Metastable flux to the probe

Metastable flux to the probe is given [1] by

$$\Gamma_m = n_{mo} \sqrt{k T_m / 2\pi m_m}, \quad (5)$$

where  $k$ ,  $T_m$ ,  $m_m$ , and  $n_{mo}$  are the Boltzmann's constant, temperature, mass, and the density of the metastable atoms in the bulk plasma, respectively. Eq.(5) is used, when the ion sheath thickness is smaller than the mean free path  $\lambda_m$  of metastable atom, for  $p > 1 \text{ Torr}$ . However, the collisionless

sheath thickness dependent metastable flux to the probe for thin and thick sheath will be discussed briefly.

### 3.3. Thin ion sheath model

The metastables density is obtained [4] from

$$D_m \nabla^2 n_m + v_m n_e - \alpha_{ci} n_e n_m = 0, \quad (6)$$

where  $n_i$  is the density of ions,  $v_m$  and  $\alpha_{ci}$  are the electron impact excitation to the metastable level frequency and the cumulative ionization rate coefficient; and  $D_m$  is the diffusion coefficients of metastable atoms, respectively. For  $n_m(0) = 0$ , and  $n_m(\infty) = n_{mo}$ ; solution of Eq.(6) for cylindrical coordinate in axial direction is

$$n_m = n_{mo} \{ \sinh(z/s_o) - 2 \sinh^2(z/2s_o) \}, \quad (7)$$

where  $z$  is the axial distance,  $s_o = \sqrt{(D_m/n_{eo}\alpha_{ci})}$  is the characteristic length of the metastable depletion zone and  $n_{eo}$  the density of electrons in bulk plasma. Taking first derivative of Eq.(7) for  $z = 0$ , we get

$$\Gamma_m = -n_{mo} \sqrt{D_m \alpha_{ci} n_{eo}}. \quad (8)$$

Putting Eq.(8) into Eq.(4), we get

$$I_{em} = -e \gamma A_p n_{mo} \sqrt{D_m \alpha_{ci} n_{eo}}. \quad (9)$$

Eq.(9) for thin ion sheath can be applied, when the ion sheath thickness is smaller than  $2s_o$ .

### 3.4. Thick ion sheath model

For thick ion sheath, Eq.(6) becomes

$$D_m \nabla^2 n_m = 0. \quad (10)$$

For  $n_m(0) = 0$  and  $n_m(s) = n_{mo}$  solution of Eq.(10) is

$$n_m = n_{mo} D_m (z/s). \quad (11)$$

For  $z = 0$ , Eq.(11) becomes

$$\Gamma_m = -D_m n_{mo} / s. \quad (12)$$

Putting Eq.(12) into Eq.(4), we get

$$I_{em} = -e \gamma A_p D_m n_{mo} / s. \quad (13)$$

$I_{em}$  can be obtained either by Eq.(9) or Eq.(13) by knowing  $\gamma$ ,  $D_m$ , and  $s$ .  $\gamma$  is estimated using a kinetic approach [5].

## 4. Theoretical model

A theoretical model is developed for  $p = 0.01 - 0.2$  Torr to calculate  $T_e$  and  $n_m$  as the functions of  $n_e$  and  $z$ .

### 4.1. Estimation of $T_e$

$T_e$  is estimated assuming Maxwellian energy distribution; the ambipolar diffusion coefficient  $D_a$ , and the direct electron impact ionization

frequency  $\nu_{di}$  depend on  $T_e$ ,  $p$ , the nature of the gas, and  $z$ . So that the charged particles is lost by  $D_a$ , which is to be balanced by  $\nu_{di}$ , under these conditions the steady state particle balance equation is

$$D_a \nabla^2 n_i + \nu_{di} n_e = 0. \quad (16)$$

Eq. (16) is solved numerically and the solution is

$$T_e = a^2 p^2 \frac{(eE_i / \sqrt{m_e})^2}{(e^z \mu_i)^2} (z/1.57)^4, \quad (17)$$

where  $a$ ,  $\mu_i$ ,  $m_e$ , and  $E_i$  are the initial slope of the ionization efficiency, mobility of ions, mass of electron, and the ionization potential of interest, respectively. Units used in Eq. (17):  $a$  [ion pairs.cm<sup>-1</sup>.Torr<sup>-1</sup>.V<sup>-1</sup>.(primary electron)<sup>-1</sup>],  $z$  [cm],  $p$  [Torr],  $E_i$  [eV],  $T_e$  [eV], and the remaining are in SI units.

### 4.2. Estimation of $n_m$

It is assumed that the ions are produced by the direct electron impact ionization of ground-, and metastable atoms, and destructed by ambipolar diffusion.  $n_i$  is obtained [4] from

$$D_a \nabla^2 n_i + \nu_{di} n_e + \alpha_{ci} n_e n_m = 0. \quad (18)$$

$n_m$  is determined from particle balance equation

$$D_m \nabla^2 n_m + v_m n_e - \alpha_{ci} n_e n_m - \alpha_q n_e n_m = 0, \quad (19)$$

where  $\alpha_q$  is the electron impact metastable quenching rate coefficient. Solutions of Eqs. (18) and (19) for the axial density profiles for ions and metastable atoms are

$$\frac{n_i}{n_e} = \frac{\nu_{di} + 0.4 \alpha_{ci} (n_m/n_e) n_{eo}}{(1.685/z)^2 D_a}, \quad (20a)$$

$$\frac{n_m}{n_e} = v_m \{ (1.456/z)^2 D_m - 0.4 n_{eo} (\alpha_{ci} + \alpha_q) \}^{-1}. \quad (20b)$$

Eqs. (20) are used for the estimation of metastable density profiles as the functions of  $n_e$ ,  $z$  and  $T_e$  for different  $p$ , taking  $T_g = 300K$ . It is assumed [6] that  $4^3P_2^0$  for Ar, and  $2^3S_1$ , and  $2^1S_0$  for He are the dominant metastable atoms in the discharge.

## 5. Experimental setup

Figure 1 shows the schematic of the discharge chamber and the probe setup. The cylindrical discharge chamber is made of stainless steel of 34.3 cm diameter and 28 cm height. Microwave power was fed to the discharge chamber by a coaxial cable. A 2.45 GHz microwave generator

with a power of 1.5 kW was used to produce discharges. A single Langmuir probe, 0.49 mm diameter, and 1 mm long, embedded in insulation with an alumina tube, was used to measure the probe characteristics. Probe was made of copper wire, and coated (thickness  $1 \mu\text{m}$ ) with silver. The probe was placed at different axial positions in the discharge chamber to measure the probe characteristics.

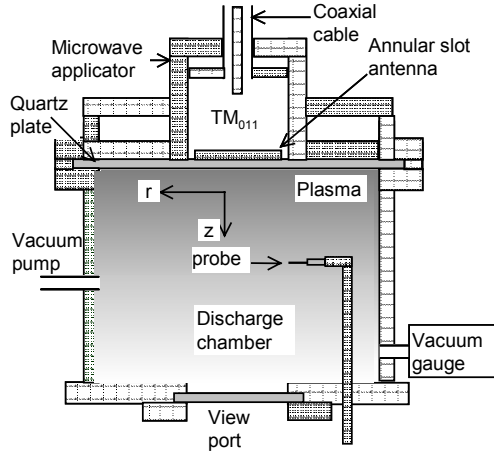


Fig 1. Schematic of the discharge chamber

## 6. Probe data analyses

Firstly, the positive part of the probe characteristics is fitted to determine  $n_e$  and  $T_e$ , because these values are used for fitting the negative part of probe data to determine  $n_m$ . A linear portion is selected for fitting. Because in this region  $I_{em}$  is independent of  $V_p$  in the positive potential region but  $I_e$  is a function of  $V_p$  and  $T_e$ . Under this condition Eq. (2) is used, together with Eq. (9), to fit the probe data iteratively and the best-fitted curve provides  $T_e$  and  $n_e$ . Secondly, the negative part of the probe characteristics is fitted taking  $T_e$  and  $n_e$  values obtained from Eq. (3) together with Eq. (13) for the determination of  $n_m$  assuming that the quasi-neutrality condition prevailed in the discharge.

## 6. Results and discussion

Figure 2 shows the experimental results for axial  $n_e$  profiles in Ar and He. In both cases,  $n_e$  decreases with increasing  $z$  from the quartz plate because of decreasing energy of the microwave field. On the other hand,  $n_e$  increases with  $p$  due to increasing electron neutral collision frequency.  $n_e$  in Ar is more than three times higher than that

of He for the same microwave power. The reason is that  $\alpha_{di}$  for Ar is much higher than that for He, as a result more ionizing events occur, and consequently more ions produced for the same microwave power in Ar.

The lines and marks in Fig.3 indicate the calculated and experimental results both for Ar, and He for axial profiles of  $T_e$  at different experimental conditions, respectively. The measured values of  $T_e$  are multiplied by 0.98, 1.14, and 1.32 for Ar, and by 1.63, 1.61, and 1.48 for He for 0.03, 0.05, and 0.10 Torr, respectively. The corresponding difference in  $T_e$  between model calculation and measurement are 2.35%, 12.5%, and 24% for Ar, and 39%, 38%, and 32% for He, respectively. These discrepancies may arise from model calculation; because only direct electron impact ionization is used in the model for simplicity neglecting other ionization processes involve for sustaining discharges. On the other hand, due to the increase of  $n_m$  with  $p$ , more ionizing events occur through cumulative, and metastable-metastable collision processes in the discharge volume, and hence calculated  $T_e$  become higher compared to those of measured values. Both in Ar, and He,  $T_e$  decrease with increasing  $p$ , and  $z$ . The electron-neutral collision frequency for momentum transfer increases with  $p$ , and consequently the electrons lose their energies. Furthermore, for the same  $p$ , the energy of the electromagnetic field is reducing with increasing  $z$  and hence  $T_e$  is decreasing.

Figure 4 shows the model calculations, and experimental results for axial  $n_m$  distribution profiles in Ar, and He, for different  $p$ . For Ar, experimental  $n_m$  are multiplied by 1.12, 2.34, and 1.87, and for He, these are 3.05, 3.03, and 1.09 respectively, for 0.03, 0.05, and 0.10 Torr. These multipliers indicate that the calculated  $n_m$  are higher than those of measured  $n_m$  by 11%, 57%, and 46% for Ar, and by 67%, 67%, and 8% for He, respectively, for 0.03, 0.05, and 0.10 Torr. These discrepancies of  $n_m$  between the measurement and calculation may arise due to the changes in  $\gamma$ ,  $z$ ,  $T_e$ ,  $T_m$ , the cross section data used in the modeling, and the collision processes involved in the discharge. Firstly, the values of  $\gamma$  for dirty surface are more than two times higher [7] than that for clean surface.  $\gamma$  used in the model calculation are for clean surface, while in the experiment the probe surface can be contaminated.

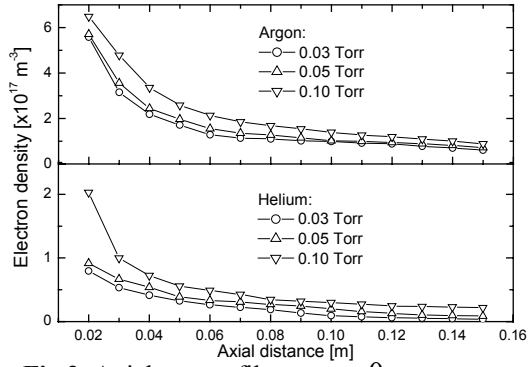


Fig 2. Axial  $n_e$  profiles at  $r = 0$ .

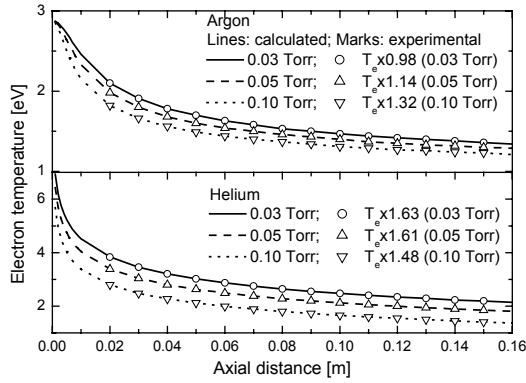


Fig 3. Axial  $T_e$  profiles at  $r = 0$ .

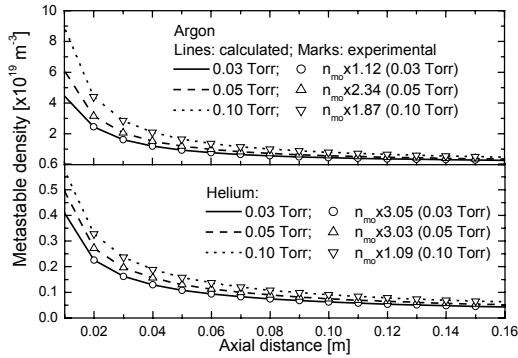


Fig 4. Axial  $n_m$  profiles at  $r = 0$ .

So that surface contamination can largely affect experimental  $n_m$  values. Secondly, it was found from model calculation that 1mm difference in  $z$ , such little displacement in positioning probe may take place during probe setup, includes 10% variation on measured  $n_m$ . Thirdly,  $n_m$  is inversely proportional to the square root of  $T_m$ ; it is found that  $n_m$  is almost double at 1000K with respect to that at 300K. The assumed  $T_m$  may not practically prevail in the plasma and hence  $n_m$  can be changed with  $T_m$ . Fourthly, calculated  $T_e$  are in average 13% higher than those of measured values; and  $\alpha_m$  is an exponential function of  $T_e$ .

So that a little change of  $T_e$  causes a large change in  $\alpha_m$  will produce a significant variation in  $n_m$ . The remaining sources for  $n_m$  discrepancies mentioned above are less significant. Hence, due to the above-mentioned causes the discrepancies of  $n_m$  between calculation and measurement can easily be introduced. It is also seen from Fig. 4 that  $n_m$  decreases with increasing  $z$ . Because  $\alpha_m$  decreases due to decreasing  $T_e$  with increasing  $z$ , and as a result  $n_m$  reduces. On the other hand,  $n_m$  increases with  $p$  because of increasing  $\nu_m$ .

## 7. Conclusion

Experimental results are compared with model calculation.  $n_e$  decreases with increasing  $z$  from the quartz plate because of decreasing energy of the microwave field. On the other hand,  $n_e$  increases with  $p$  due to increasing  $\nu_{di}$ . Differences of  $n_e$  between measurement and model prediction can arise due to the discrepancies of  $T_e$ .  $n_m$  reduces with increasing  $z$  due to decreasing  $T_e$  with  $z$ , and  $n_m$  increase with  $p$  due to increasing  $\nu_m$ . The discrepancies of  $n_m$  between measurement and model prediction arise due to the changes in  $\gamma$ , probe positioning,  $T_e$ , and  $T_m$ . However, model predictions compare favorable with the experimental results.

## References

- [1] Kagan Yu M and Perel V I, *Sov Phys: Uspekhi* **6** (1964) 767.
- [2] Hagstrum H D, *Phys Rev*, **96** (1954) 336.
- [3] Ye M Y, and Takamura S, *Phys Plasmas*, **7** (2000) 3457.
- [4] Delcroix J L, Ferreira C M and Ricard A 1976 *Principles of Laser Plasma*, ed G Bekefi (NY: Wiley, NY) Chapter 3.
- [5] Nagorny V P and Drallos P J, *Plasma Sources Sci Technol*, **6** (1997) 212.
- [6] Y.P. Raizer, *Gas Discharge Physics*, Springer-Verlag (1991).
- [7] Phelps A V, Petrovic Z Lj, *Plasma Sources Sci Technol*, **8** (1999) R21.